A Bidirectional Energy Conversion Circuit Toward Multifunctional Piezoelectric Energy Harvesting and Vibration Excitation Purposes

Bao Zhao, *Graduate Student Member, IEEE*, Jiahua Wang, Wei-Hsin Liao, *Senior Member, IEEE*, and Junrui Liang, *Senior Member, IEEE*

***Abstract*—Piezoelectric transducers provide a bidirectional channel for converting energy from mechanical form to electrical or in the opposite direction. Various applications were developed with either of these two energy-flow processes. For example, energy harvesters take advantage of the energy flow from mechanical to electrical domains, while vibration exciters utilize that from electrical to mechanical domains. However, few designs have integrated the bidirectional energy-flow processes in a single device in the past. Such an integration is beneficial to some multifunctional applications. The key obstacle of integrated bidirectional design results from the interface circuit design, rather than the transducer. This article makes a breakthrough by proposing a bidirectional energy conversion circuit (BECC) solution for the time-sharing energy harvesting and vibration exciting purpose. It is realized by developing a new control strategy on the synchronized triple bias-flip (S3BF) piezoelectric interface circuit, which was formerly used for energy harvesting enhancement. The control logic for energy harvesting and vibration exciting modes are discussed in detail. The time-sharing multi-functional ability is validated in experiments. It is the first time to realize a compact and integrated self-excitable energy harvester by using a single interface circuit. Experiments are carried out for validating the feasibility of the BECC toward future versatile engineering designs.**

***Index Terms*—Bidirectional energy conversion, energy harvesting (EH), piezoelectric, vibration excitation (VE).**

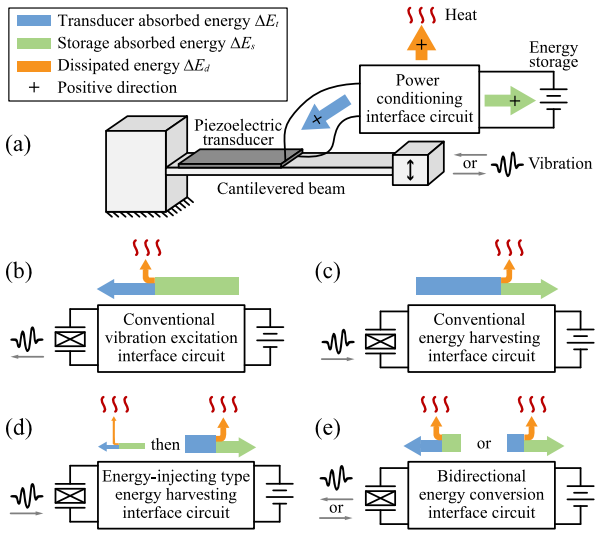

Fig. 1. Energy flow in different types of piezoelectric interface circuits. (a) Piezoelectric device with general energy flows. (b) Conventional vibration excitation circuit. (c) Conventional energy harvesting circuit. (d) Energy-injecting type energy harvesting circuit. (e) Bidirectional energy conversion circuit, whose concept is implemented in this study.

I. Introduction

THE direct and converse piezoelectric effects have been studied and utilized over the last century since the discovery of piezoelectricity in 1880 [2]. Given the coupling feature of the piezoelectric materials, which incorporates mechanical and electrical energy and variables, those materials have been used in many engineering applications, such as pressure sensors, micropositioning actuators, etc. Recently, with the development of Internet of things, piezoelectric energy harvesting (PEH) technology has received more research interests toward vibration-powered wireless sensor networks [3]. Efficient and flexible power conversion can be achieved by using some sophisticated power electronics. On the other hand, by adopting the switching power converter concept, novel multifunctional piezoelectric interface circuits can also be implemented.

In a general piezoelectric device, as shown in Fig. 1(a), there are three possible energy flows, which are absorbed by the piezoelectric transducer (denoted as ΔE_t), the electrical energy storage (ΔE_s), or dissipated by the parasitic resistance during power conditioning (ΔE_d). Regardless of the function of the device, the conservation of energy holds within these three energy flows, i.e.,

$$\Delta E_t + \Delta E_s + \Delta E_d = 0. \tag{1}$$

Manuscript received September 24, 2020; revised March 2, 2021 and April 3, 2021; accepted May 15, 2021. Date of publication May 26, 2021; date of current version July 30, 2021. This work was supported in part by the Natural Science Foundation of Shanghai under Grant 21ZR1442300, in part by the ShanghaiTech University under Grant F-0203-13-003, and in part by the Shanghai Key Laboratory of Mechanics in Energy Engineering under Grant ORF-202001. This article is an extended version of the paper presented at the 2019 SPIE Smart Structures + Nondestructive Evaluation Conference [1]. Recommended for publication by Associate Editor B. Semail. *(Corresponding authors: Wei-Hsin Liao; Junrui Liang.)*

Bao Zhao and Junrui Liang are with the School of Information Science and Technology, ShanghaiTech University, and Shanghai Engineering Research Center of Energy Efficient and Custom AI IC, Shanghai 201210, China (e-mail: zhaobao@shanghaitech.edu.cn; liangjr@shanghaitech.edu.cn).

Jiahua Wang and Wei-Hsin Liao are with the Department of Mechanical and Automation Engineering, Chinese University of Hong Kong, Hong Kong (e-mail: wangjiahua@link.cuhk.edu.hk; whliao@cuhk.edu.hk).

Color versions of one or more figures in this article are available at https://doi.org/10.1109/TPEL.2021.3083256.

Digital Object Identifier 10.1109/TPEL.2021.3083256

ΔE_t and ΔE_s is either positive or negative, i.e., the corresponding energy flow can be bidirectional. ΔE_d is always positive because the dissipated heat can return to neither mechanical nor electrical energy in these systems. Fig. 1(b)–(e) shows the energy flow illustrations of four types of typical piezoelectric interface circuits, which are specified for different application purposes. They realize different functions by utilizing either or both of the forward and backward piezoelectric energy conversions.

Fig. 1(b) illustrates the energy flows in a conventional vibration excitation (VE) circuit. The transducer absorbs positive energy, while the storage device absorbs negative energy. It means that the energy is extracted from the storage and injected into the transducer for producing mechanical vibration. This type of actuator driving circuits are used in the driver module of piezoelectric transformers [4], piezoelectric based microrobots [5]–[7], and other piezoelectric actuators for positioning [8], [9]. On the other hand, in the energy harvesting (EH) applications, the main energy flow is in the opposite direction, i.e., from the transducer to storage. Fig. 1(c) shows the energy flows in a conventional PEH interface circuit. The most investigated PEH interface circuits include the standard EH bridge rectifier [10], synchronized switch harvesting on inductor (SSHI) [11], synchronous electric charge extraction [12], etc. In these conventional PEH circuits, energy flows unidirectionally from the transducer to the electrical storage device. Some active EH schemes such as the synchronized multiple bias-flip (SMBF) interface circuit have emerged since 2010 [13]–[18]. In these new circuits, the energy flows are different from the conventional PEH system. Besides energy extraction from the transducer at every synchronized instant, energy injection back to the transducer is implemented with specific amounts at specific instants in order to enhance the overall EH capability. Recently, some inductorless switched-capacitor integrated circuit solutions have been proposed to meet the miniaturization requirement [19], [20]. The energy flow of the energy-injecting-type PEH circuit is shown in Fig. 1(d). Both the conventional PEH circuits and the energy-injecting-type PEH circuits focus on extracting energy from the transducer and storing it in a stable electrical form in the storage device. However, compared with the conventional PEH circuit, the energy-injecting one puts a small portion of the harvested energy back to the transducer, whose method was called prebiasing [14] or energy investment [16] in some papers, in order to get more return in the long run. Due to the mutual exclusion of the two forward mechanical-to-electrical and backward electrical-to-mechanical energy flows, the previous designs of EH circuits and VE circuits have little crossover. However, recently, there are some applications beckoning for an integration of the two energy-flow processes to realize multifunctional applications. For one example, in some nonlinear EH applications, the vibration boosting mechanism is needed for pushing the vibration from low-energy orbit to high-energy orbit [21]–[23], in order to harvest more energy under the same VE. For another example, in some nondestructive evaluation (NDE) applications, piezoelectric energy harvesters are used to generate Lamb wave and sense structural vibration [24], [25]. Guyomar *et al.* proposed the concept of self-powered autonomous wireless transmitters/receivers system for NDE purpose [26], which also incorporated the EH function. In their design, the EH and VE functions were realized by different circuits modules and separate piezoelectric elements. By introducing the new design concept of bidirectional energy conversion circuit (BECC), different time-sharing functions might be integrated someday toward self-powered, self-contained, and fully autonomous multifunctional devices. The energy flow of the BECC is illustrated in Fig. 1(e). The idea of the BECC is not to violate the conservation of energy by making the forward and reverse energy flows simultaneously, but to implement either of these two energy-flow processes in some specific and separated time intervals. Such operation is usually referred to as *time-sharing operation*. In one of the authors' study about the nonlinear EH system, they have demonstrated that the time-sharing EH and VE helps build a self-contained and flexible nonlinear energy harvester [1], [27], where the high-energy orbit vibration is excited by the same EH circuit, rather than additional electrical or mechanical modules.

There were some multifunctional piezoelectric design by combining the sensing and actuation functions [28] or sensing and EH functions [29], [30]. However, to the best of the authors' knowledge, no one combined the two-way piezoelectric energy conversions in a single power converter circuit. It should be noticed that the recent limitation against the realization of the bidirectional energy conversion is not caused by the piezoelectric transducer, but the interface circuit. In this article, the investigation of the BECC starts from a recently proposed energy-injecting harvesting circuit, the synchronized triple bias-flip (S3BF) circuit [31], [32]. Based on the same S3BF topology but carrying out a different switching control strategy, the time-sharing EH and VE functions are realized by using a single interface circuit. Such an integrated BECC circuit might lead to the inventions of more piezoelectric multifunctional solutions, which benefit the designs of nonlinear energy harvesters [33], vibration-powered NDE devices [34], etc., in the future.

II. Principle

The general SMBF circuit model was developed with the purpose of optimizing the strategy of active energy injection (also called energy investment [16] or prebiasing [14]) toward better EH capability [17]. The theory has led to the inventions of parallel-S3BF (P-S3BF) [18], parallel-S7BF [35], and series-S3BF (S-S3BF) [32] interface circuits, which increase the harvested power under the same excitation. The general SMBF model includes two categories: the parallel and series SMBF circuits [17]. The parallel type uses a bidirectional switch branch for bias-flip and a unidirectional bridge rectifier for harvested energy collection. On the other hand, the series type only uses a bidirectional switch branch for both bias-flip and energy storage purposes. Theoretically speaking, the parallel circuits outperforms their series counterparts, in terms of EH capability [17]. However, given its unique feature of fully bidirectional energy conversion between the piezoelectric transducer and the storage capacitor, the series SMBF topology is more suitable to be further developed into a general BECC.

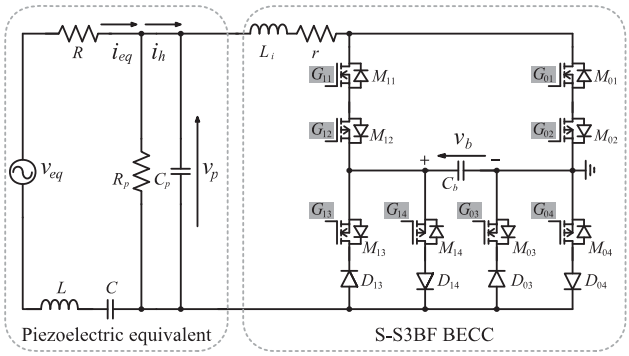

Fig. 2. S3BF BECC circuit topology.

A. Circuit Topology

The proposed BECC solution studied in this article is developed based on an S-S3BF piezoelectric interface circuit [17], [32], whose topology is shown in Fig. 2. In Fig. 2, the left portion represents the equivalent lumped dynamic model of a piezoelectric structure near the first vibration mode. The piezoelectric equivalent includes six components. An equivalent voltage source v_{eq} is proportional to the excitation force. Equivalent resistance R, inductance L, and capacitance C represent the mechanical dynamics of damping, mass, and stiffness, respectively. C_p and R_p denote the piezoelectric clamped capacitance and shunt leakage resistance, respectively. The current flowing through the RLC branch is marked as $i_{\text{eq}}(t)$. It is proportional to the vibration velocity. Given that $\omega C_p R_p \gg 1$ in most cases, where ω is the vibration frequency, we have $i_{\text{eq}} \approx i_h$. The right portion of Fig. 2 is the S-S3BF interface circuit. It is an inductive current-steering switch network, which controls the charging or discharging behavior of the bias capacitance C_b. The switch network is composed of eight power MOSFETs and four diodes for properly enabling specific current flows under different operation modes. In each switch branch, two transistors M_{x1} and M_{x2} ($x = 0$ or 1) form a bidirectional switch, M_{x3} and D_{x3} form the upward current path, and M_{x4} and D_{x4} form the downward one. The capacitor C_b connects the middle points of the two switch cells. C_b is not only used to provide bias-voltage references during each bias-flip action but also acts as energy storage in EH modes and power supply in energy exciting modes.

There are totally eight switch transistors in the S-S3BF interface circuit. It provides more degrees of control freedom toward a multifunctional interface circuit. Nevertheless, in the previous studies, which only focused on EH, the potential of S-S3BF was not fully revealed. New control methods are proposed and implemented in this article to make S-S3BF into a more general BECC.

The control logic of different operation modes and their corresponding switch conducting paths are summarized in Table I and illustrated in Fig. 4. In Table I, "P" represents a complete bias-flip phase. The subscripts denote the bias voltage and current directions of a specific bias-flip action. "p1," "0," or "n1" represent the bias voltage of V_b, 0, or $-V_b$, respectively; "dn" or "up" represent the enabled downward or upward current flow direction, respectively. The current flows of all six possible bias-flip actions in the S3BF BECC are shown in Fig. 4. By properly controlling the switching sequence at each synchronized instant (zero-crossing point of vibration velocity or i_{eq}), a sophisticated current flow can be produced through the piezoelectric capacitance C_p. The operation modes of EH and VE at different levels can be implemented by taking the bias-flip actions according to the action orders listed in Table I.

TABLE I
SWITCH CONTROL OF THE BECC UNDER DIFFERENT OPERATION MODES

Operation mode	Bias-flip actions at i_{eq} falling edge	Bias-flip actions at i_{eq} rising edge
S1BF-EH	$\text{P}_{\text{p1,dn}}$	$\text{P}_{\text{n1,up}}$
S3BF-EH	$\text{P}_{\text{p1,dn}} \rightarrow \text{P}_{\text{0,dn}} \rightarrow \text{P}_{\text{n1,dn}}$	$\text{P}_{\text{n1,up}} \rightarrow \text{P}_{\text{0,up}} \rightarrow \text{P}_{\text{p1,up}}$
S1BF-VE	$\text{P}_{\text{p1,up}}$	$\text{P}_{\text{n1,dn}}$
S3BF-VE	$\text{P}_{\text{p1,up}} \rightarrow \text{P}_{\text{n1,dn}} \rightarrow \text{P}_{\text{p1,up}}$	$\text{P}_{\text{n1,dn}} \rightarrow \text{P}_{\text{p1,up}} \rightarrow \text{P}_{\text{n1,dn}}$

B. S1BF-EH Mode

The S1BF-EH mode realizes the function of series-SSHI [11]. Each cycle can be divided into four working phases H1-1–H1-4, as shown in Fig. 3(a). Its waveform and the enlarged view of the downstairs bias-flip instant are shown in Fig. 3(a)–(c). H1-1 and H1-3 are open-circuit phases, while H1-2 and H1-4 are downstairs and upstairs bias-flip phases, respectively. The horizontally enlarged view of the H1-2 phase is shown in Fig. 3(b). There is only one bias-flip action in this phase. Once the piezoelectric current i_{eq} crosses zero from a positive to a negative value, the piezoelectric voltage v_p is flipped with respect to the bias voltage v_b from V_0 to V_1 by conducting the circuit branches highlighted in red in Fig. 4(a), which is denoted as $\text{P}_{\text{p1,dn}}$ bias-flip action in Table I. The storage capacitance C_b is selected much larger than the piezoelectric capacitance C_p for filtering and storage purposes. Its voltage level gradually rises under the harvesting (passive [17]) bias-flip action. Fig. 3(c) shows the vertically enlarged view of the storage voltage v_b. On the other hand, the upstairs bias-flip action in phase H1-4 is denoted as $\text{P}_{\text{p1,up}}$, whose conducting branches are shown in Fig. 4(d).

The relation of the intermediate voltages V_0 and V_1 and energy breakdown in the S1BF-EH mode can be regarded as a special case of the S3BF-EH mode, in which the second and third bias-flip actions are muted. Therefore, the formula of voltage relation in S1BF-EH mode can be integrated in (2)–(5).

C. S3BF-EH Mode

The S3BF-EH mode realizes the function of S-S3BF [32]. Fig. 3(d) shows the general waveform in this mode. Each cycle can be divided into eight working phases H3-1–H3-8. The horizontally enlarged view of the downstairs synchronized instant is shown in Fig. 3(e). Each phase out of H3-2–H3-4 includes a bias-flip action $\text{P}_{\text{p1,dn}}$, $\text{P}_{\text{0,dn}}$, or $\text{P}_{\text{n1,dn}}$, respectively. The corresponding conducting branches in the three actions are shown in Fig. 4(a)–(c), respectively. There are four intermediate voltages from V_0 to V_3, as shown in Fig. 3(e). After nondimensionalized with respect to the open-circuit voltage V_{oc}, e.g., $\tilde{V}_0 = V_0/V_{\text{oc}}$,

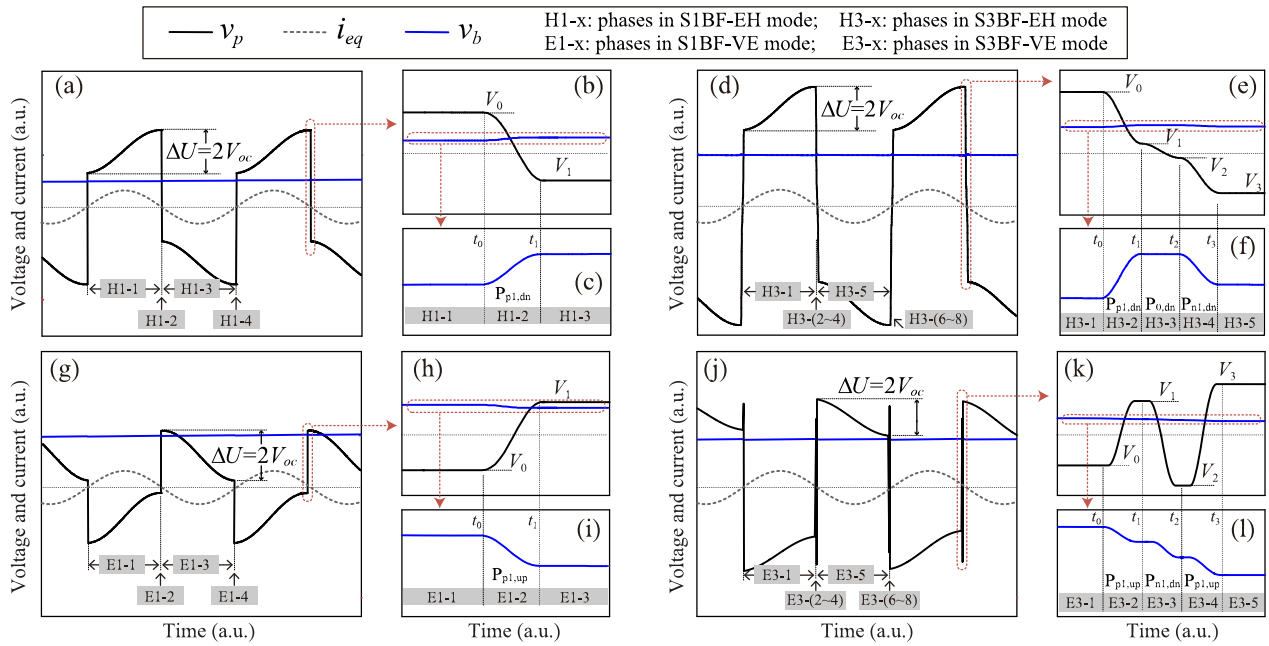

Fig. 3. Waveform in different operation modes. (a)–(c) S1BF-EH. (d)–(f) S3BF-EH. (g)–(i) S1BF-VE. (j)–(l) S3BF-VE.

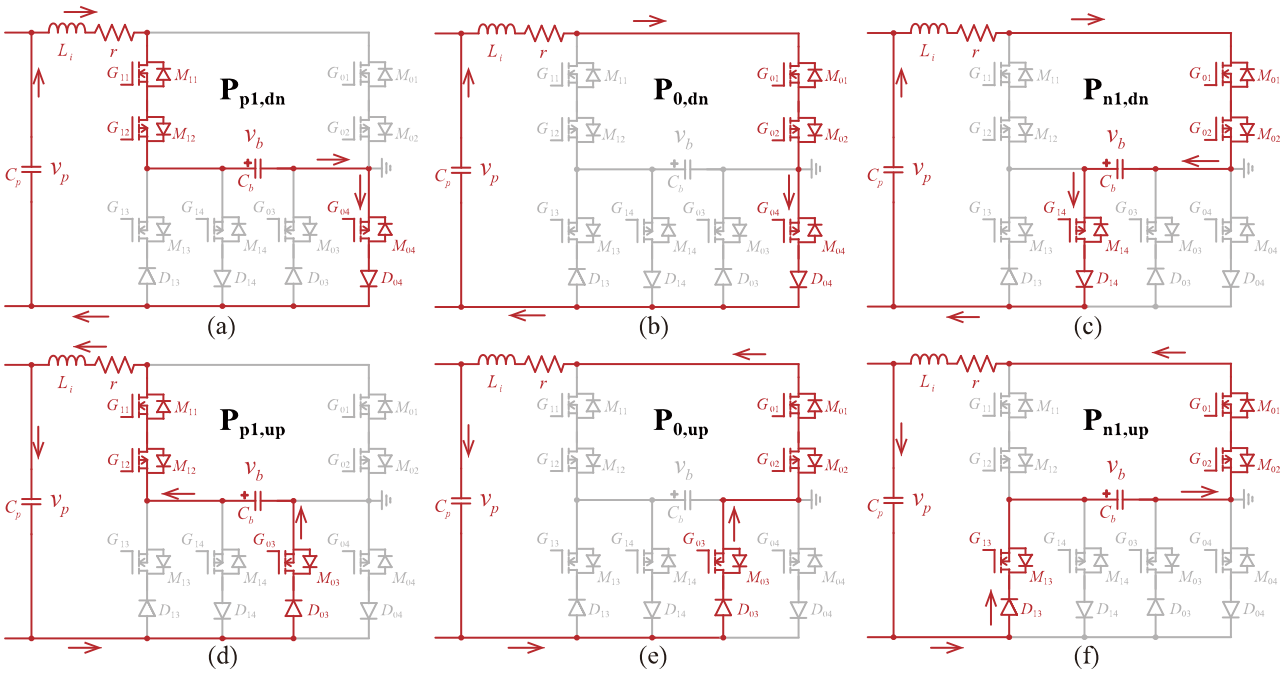

Fig. 4. (a)–(f) Conducting circuit branches in six bias-flip actions.

the relationship among $\tilde{V}_0$, $\tilde{V}_1$, $\tilde{V}_2$, and $\tilde{V}_3$ can be expressed as follows:

$$\begin{bmatrix} 1 & & & 1 \\ \gamma_1 & -1 & & \\ & \gamma_2 & -1 & \\ & & \gamma_3 & -1 \end{bmatrix} \begin{bmatrix} \tilde{V}_0 \\ \tilde{V}_1 \\ \tilde{V}_2 \\ \tilde{V}_3 \end{bmatrix} = \begin{bmatrix} 2 \\ (\gamma_1 - 1)\tilde{V}_b \\ 0 \\ (1-\gamma_3)\tilde{V}_b \end{bmatrix} \tag{2}$$

where $\tilde{V}_b$ is the nondimensionalized bias voltage and γ_1–γ_3 are the flipping factors (also called inversion factor in some previous studies) of the three bias-flip actions, respectively. The circuit might operate at the S1BF, S2BF, or S3BF modes under heavy-, medium-, and light-load conditions, respectively [32]. Fig. 5(a) illustrates the four intermediate voltages $\tilde{V}_m$ $(m = 0, 1, 2, 3)$ and three bias voltages $\tilde{V}_{b,m}$ under different storage voltage $\tilde{V}_b$ when

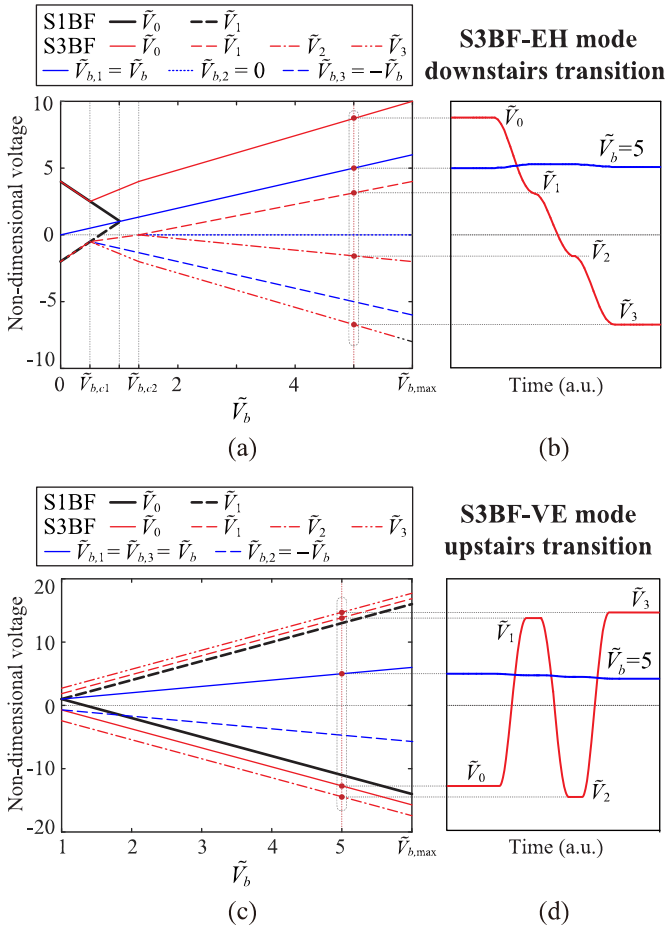

Fig. 5. Intermediate and bias voltages ($\gamma = -0.5$ for all cases). (a) S1BF-EH and S3BF-EH modes. (b) Enlarged view of intermediate voltages of the S3BF-EH mode when $\tilde{V}_b = 5$. (c) S1BF-VE and S3BF-VE modes. (b) Enlarged view of intermediate voltages of the S3BF-VE mode when $\tilde{V}_b = 5$.

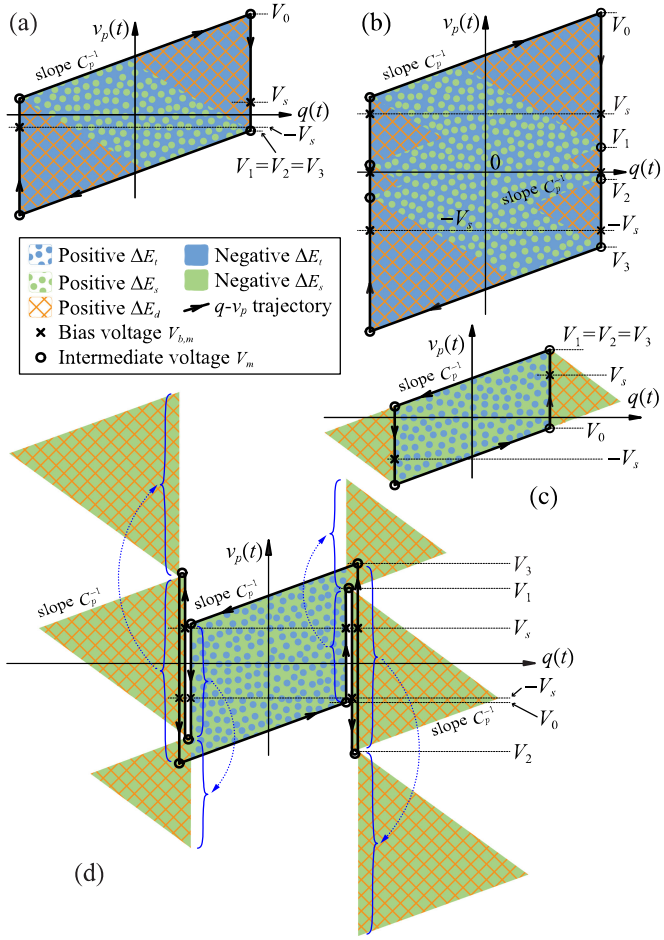

Fig. 6. Energy cycles of different operation modes. (a) S1BF-EH. (b) S3BF-EH. (c) S1BF-VE. (d) S3BF-VE.

the flipping factor $\gamma = -0.5$. The figure can be divided into three zones according to the $\tilde{V}_b$ values under different load conditions. The critical bias voltages can be formulated based on the relation among intermediate voltages at those critical conditions [18]. Besides the four phases corresponding to positive i_{eq}, there are the other four corresponding to negative i_{eq}, i.e., H3-5–H3-8. Three upstairs bias-flip actions take places in H3-6–H3-8 phases, which are denoted as $\text{P}_{\text{n1,up}}$, $\text{P}_{\text{0,up}}$, and $\text{P}_{\text{p1,up}}$, respectively. The intermediate voltages in upstairs actions are just the opposite numbers of those expressed in (2). The control logic in the S3BF-EH mode is also listed in Table I.

The S3BF-EH mode has higher EH capability than S1BF-EH due to stronger energy extraction ability and less energy dissipation in power conditioning, such as to increase the net harvested energy under the same mechanical excitation [17]. The energy relationship among extracted energy (negative transducer absorption ΔE_t), harvested energy (storage absorption ΔE_s), and dissipated energy (ΔE_d) can be illustrated with the energy cycle in the $q(t)$ versus $v_p(t)$ plane, where $q(t) = \int i_h(t)dt \approx \int i_{\text{eq}}(t)dt$ represents the electric charge. The extracted energy in one cycle corresponds to the solid blue area in Fig. 6(a) and (b), which is enclosed by the clockwise q–v_p trajectory. Therefore, the transducer extracted energy (negative absorption)[1] is formulated as follows:

$$\Delta E_t = 2C_p V_{\text{oc}} \left(V_3 - V_0\right). \tag{3}$$

Neglecting the energy dissipation of the steering diodes, the dissipated energy is mainly caused by the underdamped r–L_i–C_p branch during the bias-flip actions. The dissipated energy in each bias-flip action is illustrated with the orange criss-cross patterned area in Fig. 6(a) and (b). The total dissipated energy can be formulated as follows:

$$\Delta E_d = \sum_{m=1}^{3} C_p(1-\gamma_m^2)\left(V_{m-1} - V_{b,m}\right)^2 \tag{4}$$

According to the energy flow analysis of the PEH system [37], the net harvested energy in one cycle is the difference between energy extraction and dissipation, which corresponds to the

[1]Since the piezoelectric capacitance C_p is energy neutral in one cycle under steady state, the energy extracted by the harvesting circuit is equal to that extracted by the C_p and circuit combination. Putting C_p and the circuit together facilitates the analysis of transient bias-flip actions and steady-state equivalent impedance [36].

green dot patterned area in Fig. 6(a) and (b). The harvested energy (storage absorption) in one cycle is expressed as follows:

$$\Delta E_s = 2C_p\left[(V_0 - V_1) - (V_2 - V_3)\right]V_b. \tag{5}$$

According to (1), the sum of (3)–(5) should equal to zero, such that the conservation of energy holds. Equations (3)–(5) are also applicable to S1BF-EH by setting a special case $\gamma_1 = \gamma$ and $\gamma_2 = \gamma_3 = 1$. As we can observe by comparing Fig. 6(a) and (b), the harvested energy of S3BF in one cycle is larger than that in S1BF, as it can enlarge the v_p magnitude and reduce the energy dissipation by inserting more bias-flip actions in S3BF.

D. S1BF-VE Mode

In EH modes, the piezoelectric voltage v_p was made to have the same polarity of the equivalent current i_{eq}, as shown in Fig. 3(a) and (d), such that their product, the extracted power, is positive in a whole cycle. On the other hand, if we make v_p the opposite polarity of i_{eq}, as shown in Fig. 3(g) and (j), power flow reverses; the circuit operates in VE modes. The reversed energy flow is enabled by injecting energy into the resonant piezoelectric transducer at each synchronized instant. If there is only one injecting (active [17]) bias-flip action, the corresponding working mode is called S1BF-VE. The operating waveform of S1BF-VE is shown in Fig. 3(g). Each cycle includes two open-circuit phases E1-1 and E1-3, as well as one upstairs bias-flip phase E1-2 and one downstairs bias-flip phase E1-4. Take the upstairs E1-2 phase as an example; when the equivalent current i_{eq} crosses zero from positive to the negative, the branches highlighted in Fig. 4(d) will be conducted. Energy flows out from the storage capacitor C_b to charge the piezoelectric capacitor C_p. Therefore, v_p rises from negative to positive, as shown in Fig. 3(h), while v_b drops, as shown in Fig. 3(i). The gross effect of v_p and i_{eq} in opposite polarities makes the interface circuit as a synchronized voltage source; therefore, the piezoelectric structure starts to vibrate gradually. The driven force magnitude is proportional to the bias voltage v_b.

E. S3BF-VE Mode

Besides S1BF-VE, the S3BF-VE mode is also designed for achieving higher excitation level. As shown in Fig. 3(k), S3BF-VE consists of three active bias-flip actions in each synchronized instant. The open-circuit phase E3-1 and the first bias-flip action phase E3-2 are the same as E1-1 and E1-2 in the S1BF-VE mode, respectively. In order to achieve higher level excitation, S3BF-VE introduces two more bias-flip phases E3-3 and E3-4 after E3-2 to boost v_p further rising from V_1 to V_3. Given the intermediate voltages during the upstairs actions, as shown in Fig. 3(k), relationship of four nondimensionalized intermediate voltages $\tilde{V}_m$ and bias voltage $\tilde{V}_b$ can be formulated as follows:

$$\begin{bmatrix} 1 & & & 1 \\ \gamma & -1 & & \\ & \gamma & -1 & \\ & & \gamma & -1 \end{bmatrix} \begin{bmatrix} \tilde{V}_0 \\ \tilde{V}_1 \\ \tilde{V}_2 \\ \tilde{V}_3 \end{bmatrix} = \begin{bmatrix} 2 \\ (\gamma-1)\tilde{V}_b \\ (1-\gamma)\tilde{V}_b \\ (\gamma-1)\tilde{V}_b \end{bmatrix}. \tag{6}$$

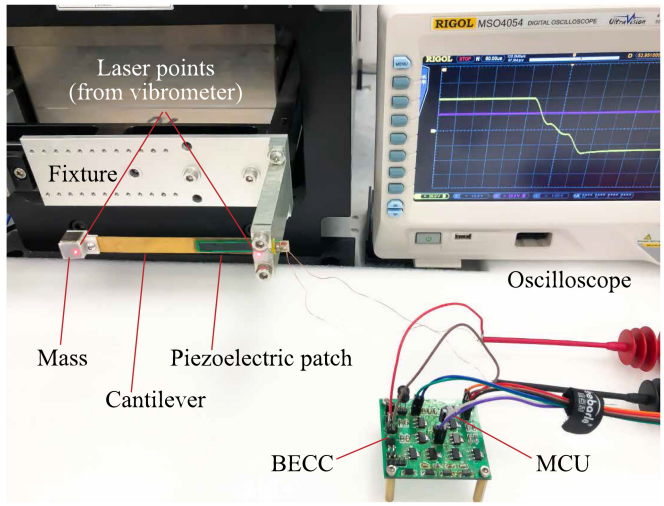

Fig. 7. Experimental setup.

When flipping factor $\gamma = -0.5$, the intermediate voltages are solved and illustrated in Fig. 5(c) as functions of bias voltage V_b. It can be seen from an enlarged case in Fig. 5(d) that the final intermediate voltage $\tilde{V}_3$ in the S3BF-VE mode is always larger than that in the S1BF-VE mode.

In the S3BF-VE mode, the transducer absorbed energy in one cycle can be formulated by using the same ΔE_t equation in (3). However, ΔE_t in the S3BF-VE mode is a positive number. It corresponds to the blue dot patterned area, which is enclosed by the counterclockwise q–v_p trajectory, in Fig. 6(c) and (d). Since there are three bias-flip actions in S3BF-VE, as S3BF-EH does, the total dissipated energy ΔE_d shares the same expression (4). But in S3BF-VE, the bias-flip actions are never muted. Therefore, $\gamma_m = \gamma$ in (4) for this case. No matter in which cases, dissipated energy is always positive. The corresponding area is also illustrated with the orange criss-cross pattern in Fig. 6(c) and (d). v_p is back and forth in the three bias-flip actions; some of the triangular dissipation areas might overlap in the diagram. We move some line segments (indicated by blue arrows), in order to clearly show the energy picture of ΔE_d.

The storage absorption is negative in this S3BF-VE case, but the energy relation (1) still holds. Therefore, we can formulate the storage absorption as follows:

$$\Delta E_s = 2C_p\left[(V_0 - V_1) - (V_1 - V_2) + (V_2 - V_3)\right]V_b. \tag{7}$$

Negative ΔE_s means that energy is extracted from the storage capacitor C_b. ΔE_s can be divided into two parts: the first is injected into the transducer for producing mechanical vibration (becomes mechanical energy), while the second is dissipated in the bias-flipping actions (becomes thermal).

Given a stable $V_b > V_{oc}$, the ratio $\tilde{V}_3/\tilde{V}_1$ can be derived as follows:

$$\frac{\tilde{V}_3}{\tilde{V}_1} = \frac{2\left(\gamma^3 - \gamma\right)}{2\gamma - \tilde{V}_b\left(\gamma^3 - 2\gamma^2 + 2\gamma - 1\right)} + 1. \tag{8}$$

The ratio $\tilde{V}_3/\tilde{V}_1 > 1$ when $\tilde{V}_b > 1$. In such a case, S3BF-VE can carry out higher level VE than S1BF-VE. On the other hand, it

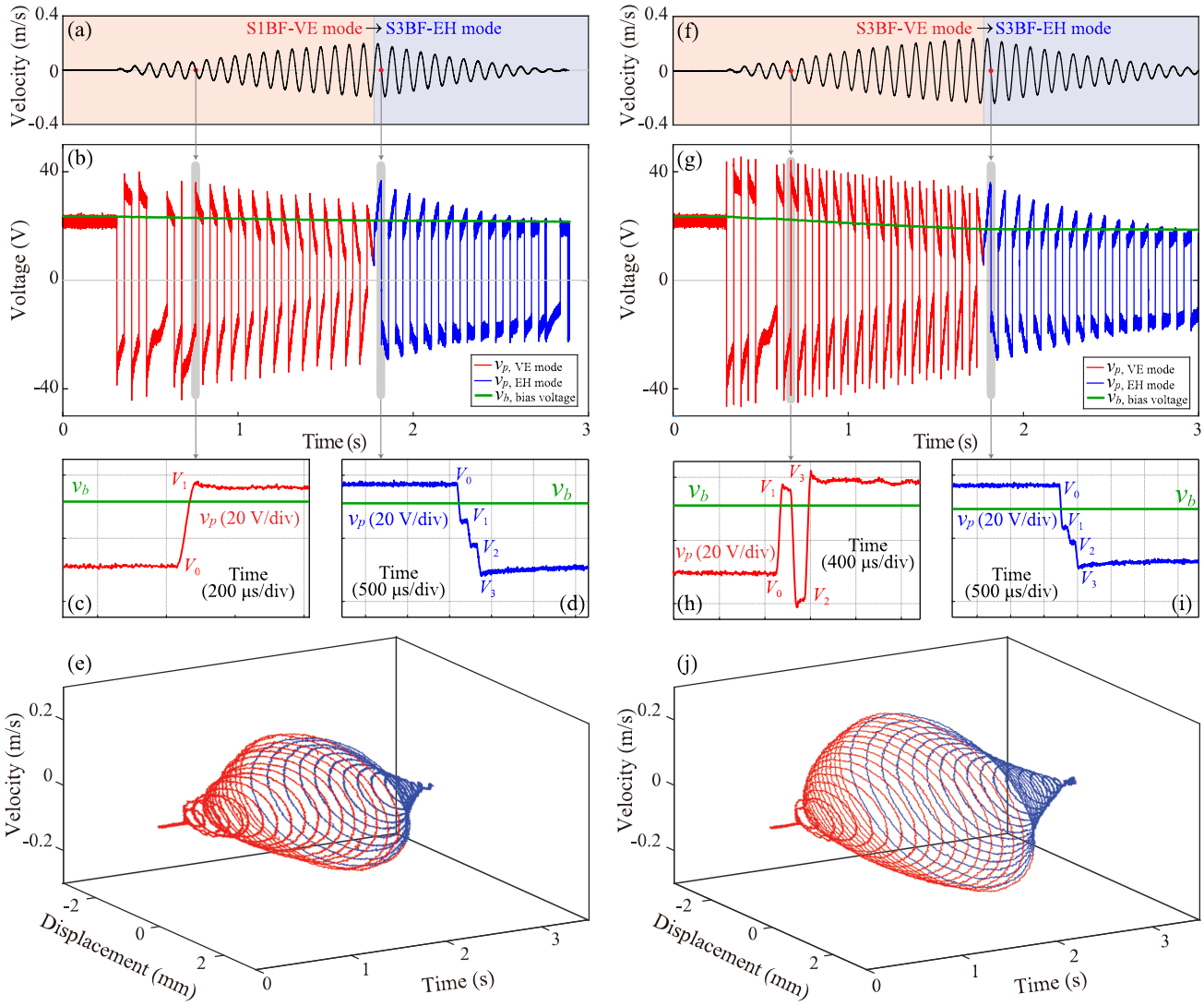

Fig. 8. Experimental results on a piezoelectric cantilever driven by the BECC interface circuit (red curves denote the VE modes, while blue ones denote the EH modes). (a)–(e) S1BF-VE to S3BF-EH operation. (f)–(j) S3BF-VE to S3BF-EH operation.

consumes much more energy than S1BF-VE does, as illustrated by the solid green pattern in Fig. 6(d). The formula and the energy picture of S1BF-VE can be easily derived according to the S3BF-VE example.

The control logic of the aforementioned four operation modes is summarized in Table I. As mentioned in Section I, the purpose of this BECC is to realize the bidirectional energy conversion and multifunctional design by properly utilizing these four basic operation modes in a time-sharing manner.

TABLE II
PARAMETERS OF A LINEAR PIEZOELECTRIC SYSTEM

Parameter	Value	Parameter	Value
M	0.009 Kg	L_i	10 mH
D	0.007 N/(m/s)	C_b	47 μF
K	52 N/m	ω	$2\pi \times 12.22$ Hz
C_p	35.75 nF	Schottky diode	SS16
R_p	1.9 MΩ	MOSFET	ZVP/ZVN 4424
γ	-0.404	k_e^2	0.007
α_e	1.13×10^{-4} N/V		

III. FUNCTION VALIDATION

Based on the control logic provided in Section II, the BECC solution is able to switch among different EH and VE modes. In order to validate the multifunctional performance of the BECC interface circuit, an experiment is carried out utilizing different operation modes in a real PEH system. Fig. 7 shows the experimental setup, while Table II lists the parameters of this setup. A piezoelectric cantilever is mounted by a fixture on a stationary base. Its output electrodes are connected to a BECC interface circuit. A laser vibrometer (OFV-552/5000, Polytec GmbH) is used to measure the velocity and the displacement of the moving tip. Since the velocity is proportional to the equivalent current i_{eq}, the velocity signal is also used for

synchronizing the bias-flip actions, which are carried out by a microcontroller (MSP430G2553, Texas Instrument) and some MOSFET switches. The microcontroller currently is powered by external batteries. Since S3BF-EH and S3BF-VE of the BECC have the same switching sequence numbers as P-S3BF does, the maximum power overhead of the switching actions is the same as that measured in [18], about 24 μW, which is lower than the harvested power. The implementation in this experiment is not an end product with self-powered capability; we focus on the functionality of the BECC first.

A storage capacitor C_b, whose capacitance is 47 μF, is used to supply energy for VE. C_b is precharged to an initial voltage of 25 V directly by a dc power source before kicking off. The beam is first excited to vibrate by implementing one of the VE modes. Then, the circuit is switched to one of the EH modes to reclaim a part of the vibration energy and, in the meanwhile, damp the vibration. Fig. 8 shows the waveform in this experiment. Fig. 8(a)–(e) corresponds to an operation from SB1F-VE to S3BF-EH. Fig. 8(f)–(j) corresponds to another operation from S3BF-VE to S3BF-EH. The experimental waveforms of vibration velocity, piezoelectric voltage v_p, bias capacitor voltage v_b, and phase portrait are recorded for showing the multifunctional ability of the BECC. The system starts from rest, i.e., zero velocity and zero displacement. At the instant of 0.3 s, there is a cold-start process, in which two voltage pulses are sent by the microcontroller to excite the beam resonance. After the cold start period, the circuit enters a VE mode, as shown by the red curves. The energy stored in C_b is gradually transformed into mechanical vibration energy. After 15 cycles of VE, the BECC is switched to an EH mode. A part of the mechanical energy is reclaimed back to the electrical form and kept in C_b. As we can see from Fig. 8(a) and (f), the beam vibration quickly damps out in the EH periods (blue segments) due to the damping effect induced by EH.

A more powerful excitation can be achieved by carrying out S3BF-VE mode operation under the same bias voltage. By implementing the S3BF-VE mode for VE, as shown in Fig. 8(h), the energy injection from C_b to the piezoelectric structure repeats three times in each synchronized instant. It produces a larger v_p magnitude across the piezoelectric transducer. Compared with the phase portrait under S1BF-VE mode operation [see Fig. 8(e)], the phase portrait under the S3BF-VE mode [see Fig. 8(j)] attains higher displacement and velocity amplitudes. Since the S3BF-VE scheme injects more energy into the system, after the same number of excitation cycles, when the circuit is switched to the S3BF-EH mode, the vibration damps out slower than the S1BF-VE case.

The voltage records of S1BF-VE, S3BF-VE, and S3BF-EH in this experiment are shown in the enlarged view of Fig. 8(c), (d), (h), and (i). Through this VE and EH experiment, the multifunctional operation and bidirectional energy conversion ability of the BECC interface circuit are validated. It is worth noting that the operation modes of the BECC can be configured flexibly. For example, when it is used in nonlinear EH cases, it can operate under S1BF-EH or S3BF-EH modes to harvest mechanical energy and use the harvested energy stored in C_b to excite the oscillator through the S1BF-VE or S3BF-VE modes. such that an orbit jump from low-energy orbit to high-energy orbit can be realized for harvesting more energy under the same base excitation [27].

IV. Conclusion

In this article, a new BECC was introduced for integrating the EH and VE functions toward a time-sharing multifunctional PEH design. It was developed based on the S3BF interface circuit via designing and implementing new control strategies. The circuit can carry out either EH or VE task in different time slots with different intensities. The circuit topology, operation principle, and energy analysis were discussed in detail. Experiments were carried out to validate the bidirectional energy conversion ability by this BECC. The proposed solution provides a new insight toward the designs of compact and multifunctional piezoelectric devices.

References

[1] B. Zhao, J. Wang, J. Liang, and W.-H. Liao, "A bidirectional energy conversion circuit for piezoelectric energy harvesting and vibration exciting purposes," *Proc. SPIE*, vol. 10967, Mar. 2019, Art. no. 109670J.

[2] J. Curie and P. Curie, "Développement par compression de l'électricité polaire dans les cristaux hémiédres à faces inclinées," *Bull. Indiana State Dept. Health*, vol. 3, no. 4, pp. 90–93, 1880.

[3] X. Li *et al.*, "ViPSN: A vibration-powered IoT platform," *IEEE Internet Things J.*, vol. 8, no. 3, pp. 1728–1739, Feb. 2021.

[4] B. Ju, W. Shao, and Z. Feng, "Piezoelectric filter module used in harmonics elimination for high-efficiency piezoelectric transformer driving," *IEEE Trans. Power Electron.*, vol. 31, no. 1, pp. 524–532, Jan. 2016.

[5] M. Karpelson, G.-Y. Wei, and R. J. Wood, "Driving high voltage piezoelectric actuators in microrobotic applications," *Sens. Actuators A. Phys.*, vol. 176, pp. 78–89, Apr. 2012.

[6] Y. Mu, T. Hu, H. Gong, L. Wang, and S. Li, "A dual-stage low-power converter driving for piezoelectric actuator applied in micro robot," *Int. J. Adv. Rob. Syst.*, vol. 16, no. 1, Jan. 2019, Art. no. 1729881419826849.

[7] M. Lok, E. F. Helbling, X. Zhang, R. Wood, D. Brooks, and G. Wei, "A low mass power electronics unit to drive piezoelectric actuators for flying microrobots," *IEEE Trans. Power Electron.*, vol. 33, no. 4, pp. 3180–3191, Apr. 2018.

[8] D. Campolo, M. Sitti, and R. S. Fearing, "Efficient charge recovery method for driving piezoelectric actuators with quasi-square waves," *IEEE Trans. Ultrason. Ferroelectr. Freq. Control*, vol. 50, no. 3, pp. 237–244, Mar. 2003.

[9] Y. Jian, D. Huang, J. Liu, and D. Min, "High-precision tracking of piezoelectric actuator using iterative learning control and direct inverse compensation of hysteresis," *IEEE Trans. Ind. Electron.*, vol. 66, no. 1, pp. 368–377, Jan. 2019.

[10] G. K. Ottman, H. F. Hofmann, A. C. Bhatt, and G. A. Lesieutre, "Adaptive piezoelectric energy harvesting circuit for wireless remote power supply," *IEEE Trans. Power Electron.*, vol. 17, no. 5, pp. 669–676, Sep. 2002.

[11] D. Guyomar, A. Badel, E. Lefeuvre, and C. Richard, "Toward energy harvesting using active materials and conversion improvement by nonlinear processing," *IEEE Trans. Ultrason. Ferroelectr. Freq. Control*, vol. 52, no. 4, pp. 584–595, Apr. 2005.

[12] E. Lefeuvre, A. Badel, C. Richard, and D. Guyomar, "Piezoelectric energy harvesting device optimization by synchronous electric charge extraction," *J. Intell. Mater. Syst. Struct.*, vol. 16, no. 10, pp. 865–876, Oct. 2005.

[13] Y. Liu, G. Tian, Y. Wang, J. Lin, Q. Zhang, and H. F. Hofmann, "Active piezoelectric energy harvesting: General principle and experimental demonstration," *J. Intell. Mater. Syst. Struct.*, vol. 20, no. 5, pp. 575–585, Mar. 2009.

[14] J. Dicken, P. D. Mitcheson, I. Stoianov, and E. M. Yeatman, "Power-extraction circuits for piezoelectric energy harvesters in miniature and low-power applications," *IEEE Trans. Power Electron.*, vol. 27, no. 11, pp. 4514–4529, Nov. 2012.

[15] M. Lallart and D. Guyomar, "Piezoelectric conversion and energy harvesting enhancement by initial energy injection," *Appl. Phys. Lett.*, vol. 97, no. 1, Jul. 2010, Art. no. 014104.

[16] D. Kwon and G. A. Rincón-Mora, "A single-inductor 0.35 μm CMOS energy-investing piezoelectric harvester," *IEEE J. Solid-State Circuits*, vol. 49, no. 10, pp. 2277–2291, Oct. 2014.
[17] J. Liang, "Synchronized bias-flip interface circuits for piezoelectric energy harvesting enhancement: A general model and prospects," *J. Intell. Mater. Syst. Struct.*, vol. 28, no. 3, pp. 339–356, 2017.
[18] J. Liang, Y. Zhao, and K. Zhao, "Synchronized triple bias-flip interface circuit for piezoelectric energy harvesting enhancement," *IEEE Trans. Power Electron.*, vol. 34, no. 1, pp. 275–286, Jan. 2019.
[19] S. Du and A. A. Seshia, "A fully integrated split-electrode synchronized-switch-harvesting-on-capacitors (SE-SSHC) rectifier for piezoelectric energy harvesting with between 358% and 821% power-extraction enhancement," in *Proc. IEEE Int. Solid-State Circuits Conf.*, 2018, pp. 152–154.
[20] Z. Chen, M.-K. Law, P.-I. Mak, W.-H. Ki, and R. P. Martins, "22.2 A 1.7 mm 2 inductorless fully integrated flipping-capacitor rectifier (FCR) for piezoelectric energy harvesting with 483% power-extraction enhancement," in *Proc. IEEE Int. Solid-State Circuits Conf.*, 2017, pp. 372–373.
[21] A. Masuda, A. Senda, T. Sanada, and A. Sone, "Global stabilization of high-energy response for a duffing-type wideband nonlinear energy harvester via self-excitation and entrainment," *J. Intell. Mater. Syst. Struct.*, vol. 24, no. 13, pp. 1598–1612, Sep. 2013.
[22] C. Lan, L. Tang, and W. Qin, "Obtaining high-energy responses of nonlinear piezoelectric energy harvester by voltage impulse perturbations," *Eur. Phys. J. Appl. Phys.*, vol. 79, no. 2, Aug. 2017, Art. no. 20902.
[23] W. Liu, Z. Yuan, S. Zhang, and Q. Zhu, "Enhanced broadband generator of dual buckled beams with simultaneous translational and torsional coupling," *Appl. Energy*, vol. 251, Oct. 2019, Art. no. 113412.
[24] Y. Liu, W. Chen, J. Liu, and S. Shi, "A cylindrical traveling wave ultrasonic motor using longitudinal and bending composite transducer," *Sens. Actuators A: Phys.*, vol. 161, nos. 1/2, pp. 158–163, 2010.
[25] G. Wang, J. Tan, Z. Zhao, S. Cui, and H. Wu, "Mechanical and energetic characteristics of an energy harvesting type piezoelectric ultrasonic actuator," *Mech. Syst. Signal Process.*, vol. 128, pp. 110–125, 2019.
[26] D. Guyomar *et al.*, "Synchronized switch harvesting applied to selfpowered smart systems: Piezoactive microgenerators for autonomous wireless transmitters," *Sens. Actuators A. Phys.*, vol. 138, no. 1, pp. 151–160, Jul. 2007.
[27] J. Wang, B. Zhao, J. Liang, and W.-H. Liao, "Orbit jumps of monostable energy harvesters by a bidirectional energy conversion circuit," in *Proc. Int. Des. Eng. Tech. Conf./Comput. Inf. Eng. Conf.*, 2019, Art. no. V00 8T10A016.
[28] S. O. R. Moheimani, "A survey of recent innovations in vibration damping and control using shunted piezoelectric transducers," *IEEE Trans. Control Syst. Technol.*, vol. 11, no. 4, pp. 482–494, Jul. 2003.
[29] Z. J. Chew, T. Ruan, M. Zhu, M. Bafleur, and J. Dilhac, "Single piezoelectric transducer as strain sensor and energy harvester using time-multiplexing operation," *IEEE Trans. Ind. Electron.*, vol. 64, no. 12, pp. 9646–9656, Dec. 2017.
[30] H. Xia, Y. Xia, Y. Ye, L. Qian, and G. Shi, "Simultaneous wireless strain sensing and energy harvesting from multiple piezo-patches for structural health monitoring applications," *IEEE Trans. Ind. Electron.*, vol. 66, no. 10, pp. 8235–8243, Oct. 2019.
[31] B. Zhao, K. Zhao, X. Wang, J. Liang, and Z. Chen, "Series synchronized triple bias-flip circuit: Maximizing the usage of a single storage capacitor for piezoelectric energy harvesting enhancement," *IEEE Trans. Power Electron.*, vol. 36, no. 6, pp. 6787–6796, Jun. 2021.
[32] R. Harne and K. Wang, "A review of the recent research on vibration energy harvesting via bistable systems," *Smart Mater. Struct.*, vol. 22, no. 2, 2013, Art. no. 023001.
[33] S. R. Anton and H. A. Sodano, "A review of power harvesting using piezoelectric materials (2003–2006)," *Smart Mater. Struct.*, vol. 16, no. 3, 2007, Art. no. R1.
[34] K. Zhao, J. Liang, and C. Chen, "Parallel synchronized septuple bias-flip circuit for piezoelectric energy harvesting enhancement," in *Proc. 43rd Annu. Conf. IEEE Ind. Electron. Soc.*, 2017, pp. 2629–2634.
[35] J. Liang and W.-H. Liao, "Impedance modeling and analysis for piezoelectric energy harvesting systems," *IEEE/ASME Trans. Mechatron.*, vol. 17, no. 6, pp. 1145–1157, Dec. 2012.
[36] J. Liang and W. H. Liao, "Energy flow in piezoelectric energy harvesting systems," *Smart Mater. Struct.*, vol. 20, no. 1, Dec. 2010, Art. no. 015005.

Bao Zhao (Graduate Student Member, IEEE) received the B.E. degree from Harbin Engineering University, Harbin, China, in 2017, and the M.E. degree from the joint program of ShanghaiTech University, Shanghai, China, and the University of Chinese Academy of Sciences, Beijing, China, in 2020.

His current research interests include energy harvesting, power electronics, and mechatronics.

Jiahua Wang received the B.E. degree in naval architecture and ocean engineering from the Dalian University of Technology, Dalian, China, in 2016, and the Ph.D. degree in mechanical and automation engineering from the Chinese University of Hong Kong, Hong Kong, in 2020.

His research interests include nonlinear energy harvesting, nonlinear orbit jumps, and electromechanical systems.

Wei-Hsin Liao (Senior Member, IEEE) received the Ph.D. degree in mechanical engineering from Pennsylvania State University, University Park, PA, USA, in 1997.

He is currently a Professor and the Chairman of the Department of Mechanical and Automation Engineering, The Chinese University of Hong Kong, Hong Kong. His research interests include smart materials and structures, energy harvesting, vibration control, mechatronics, exoskeleton, and prosthesis.

Dr. Liao is an Associate Editor for *Mechatronics*, *Journal of Intelligent Material Systems and Structures*, and *Smart Materials and Structures*. He is a fellow of the American Society of Mechanical Engineers, the Institute of Physics, and the Hong Kong Institution of Engineers.

Junrui Liang (Senior Member, IEEE) received the Ph.D. degree in mechanical and automation engineering from the Chinese University Hong Kong, Hong Kong, in 2010.

He is currently an Assistant Professor with the School of Information Science and Technology, ShanghaiTech University, Shanghai, China. His research interests include energy conversion and power conditioning circuits, kinetic energy harvesting and vibration suppression, Internet of things devices, and mechatronics.

Dr. Liang is an Associate Editor for *IET Circuits, Devices and Systems* and the General Chair of the 2nd International Conference on Vibration and Energy Harvesting Applications 2019.